Electronic Supplementary Material (ESI) for Journal of Materials Chemistry C.

Electronic Supplementary Information (ESI)

Pick your Precursor! Tailoring Size and Crystal Phase of Microwave-Synthesized sub-10 nm Upconverting Nanoparticles

Ilias Halimi,[a†] Emille M. Rodrigues,[a†] Steven L. Maurizio,[a] Hui-Qiao Tina Sun,[a] Manjot Grewal,[a] Emma M. Boase,[a] Nan Liu, [a] Riccardo Marin,[a] and Eva Hemmer* [a,b]

[a] Department of Chemistry and Biomolecular Sciences, University of Ottawa, 10 Marie-Curie Private, Ottawa (ON) K1N 6N5, Canada.

[b] Centre for Advanced Materials Research (CAMaR), University of Ottawa, Ottawa (ON) K1N 6N5, Canada.

† Authors with equal contribution

* Corresponding Author E-mail: ehemmer@uottawa.ca

Table of Content

1. Additional Experimental Details

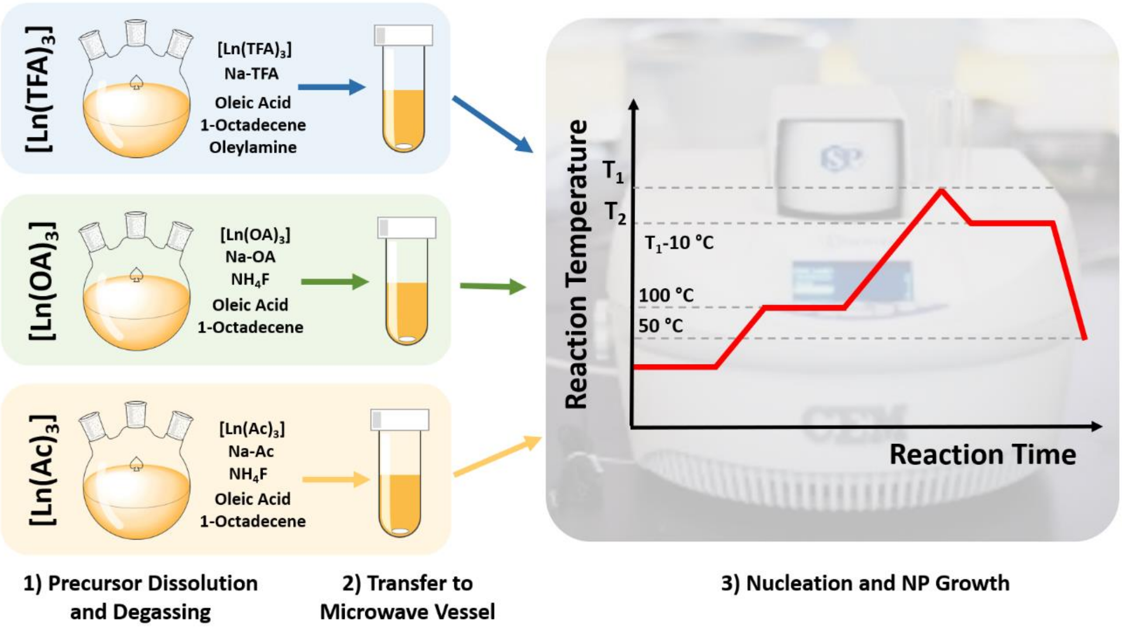

Figure S1. General scheme of the microwave-assisted synthesis of α- and β-NaGdF$_4$:Yb^{3+},Er^{3+} nanoparticles (NPs) using various Ln^{3+} precursors: [Ln(TFA)$_3$], [Ln(OA)$_3$] and [Ln(Ac)$_3$].

Table S1. Overview of the experimental conditions used in the microwave-assisted synthesis of α- and β-NaGdF$_4$:Yb^{3+},Er^{3+} nanoparticles (NPs) and their resulting approximated particle size.

Parameter Studied	**Precursor**	**Ion Ratio (Na$^+$-to-Ln^{3+})**	**Precursor Amount**	**T_1 [a]**	**T_2**	**t (T2)**	**Crystalline Phase**	**Approx. NP Size**
Precursor	[Ln(TFA)$_3$]	3:1	0.625 mmol	260 °C	250 °C	10 min	β	5.5-7.5 nm
	[Ln(Ac)$_3$]	3:1						3 nm
	[Ln(OA)$_3$]	4:1						3 nm
	[Ln(TFA)$_3$]	1:1	1.25 mmol	300 °C	230 °C	10 min	α	9.3 nm
Reaction Time	[Ln(TFA)$_3$]	3:1	0.625 mmol	260 °C	250 °C	10 min	β	5.6 nm
						1 min		4.5 nm
						1 s		3 nm
	[Ln(OA)$_3$]	4:1				10 min	β	3 nm
						1 min		3 nm
						1 s		2.6 nm
Reaction Tempe-rature	[Ln(TFA)$_3$]	3:1	0.625 mmol	270 °C	260 °C	10 min	β	5 nm
				260 °C	250 °C			5.6 nm
				250 °C	240 °C			5 nm
	[Ln(OA)$_3$]	4:1		270 °C	260 °C		β	4 nm
				260 °C	250 °C			3 nm
				250 °C	240 °C			3 nm

[a] Holding time at T_1: 1 s

2. Size and Size Distribution of β-$NaGdF_4$:Yb^{3+},Er^{3+} NPs as a Function of the Precursor

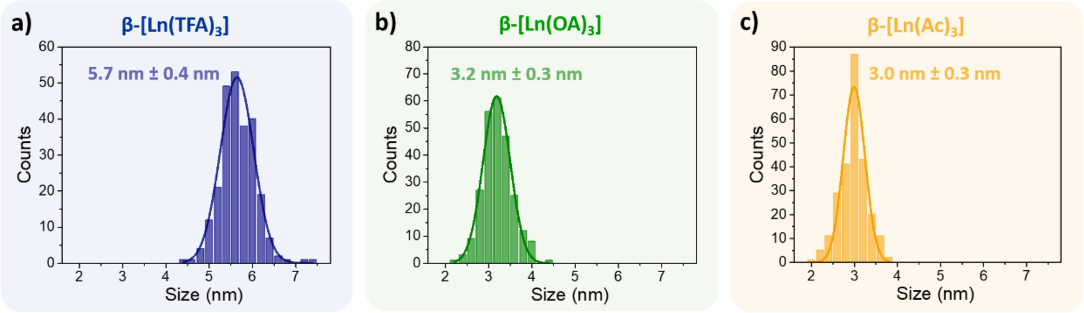

Figure S2. Mean size and size distribution of β-$NaGdF_4$:Yb^{3+},Er^{3+} NPs synthesized using a) [Ln(TFA)$_3$], b) [Ln(OA)$_3$], and c) [Ln(Ac)$_3$] as precursors. Reaction temperature T_2: 250 °C, reaction time: 10 min. The Na^+-to-Ln^{3+} ion ratio was set aiming for the hexagonal crystalline phase.

3. Structural Characterization of α-$NaGdF_4$:Yb^{3+},Er^{3+} NPs

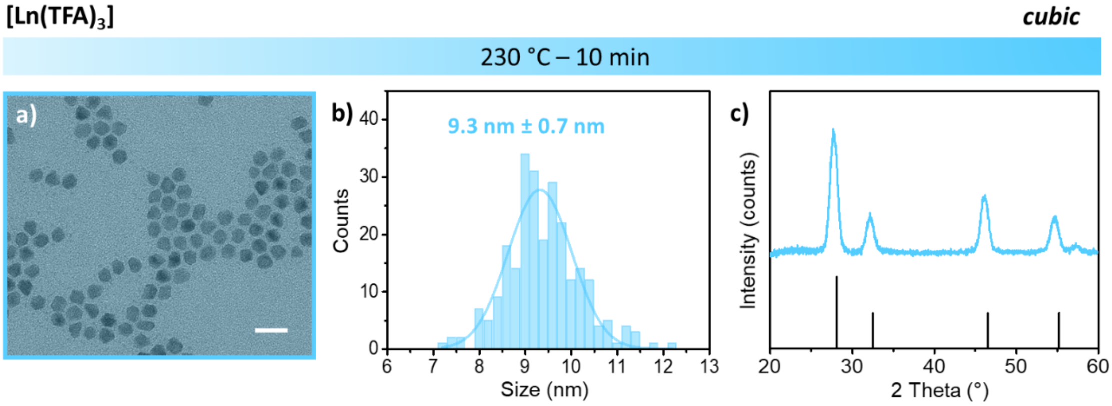

Figure S3. a) TEM image, b) mean size and size distribution, and c) XRD pattern of α-$NaGdF_4$:Yb^{3+},Er^{3+} NPs obtained by the microwave-assisted decomposition of [Ln(TFA)$_3$]. Reaction temperature T_2: 230 °C, reaction time: 10 min. The Na^+-to-Ln^{3+} ion ratio was set aiming for the cubic crystalline phase. Reference: α-$NaGdF_4$ (PDF#: 00-027-0697). Scale bar in TEM image: 20 nm.

4. XRD Patterns of Samples Exhibiting Phase Mixtures

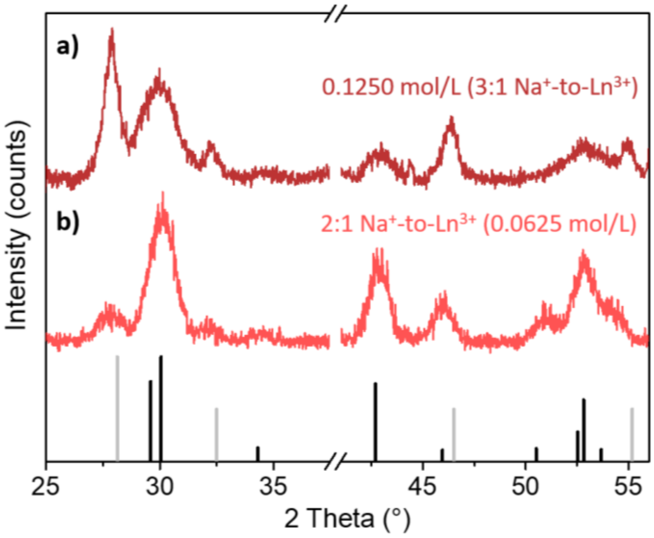

Figure S4. Effect of precursor concentration and Na^+-to-Ln^{3+} ion ratio on phase formation: a) Using a too high Ln^{3+} ion concentration (0.1250 mol/L *versus* 0.0625 mol/L) in combination with a 3:1 Na^+-to-Ln^{3+} ion ratio resulted in the formation of a phase mixture. b) Using a Na^+-to-Ln^{3+} ion ratio of only 2:1 (*versus* 3:1) led to the formation of α-$NaGdF_4$ in addition to β-$NaGdF_4$ (Ln^{3+} ion concentration: 0.0625 mol/L). References: α-$NaGdF_4$ (PDF#: 00-027-0697, light grey lines), β-$NaGdF_4$ (PDF#: 01-080-8787, black lines). Reflections at 39° due to NaF were removed for clarity.

5. Thermogravimetric Analysis (TGA) of the Used Precursors

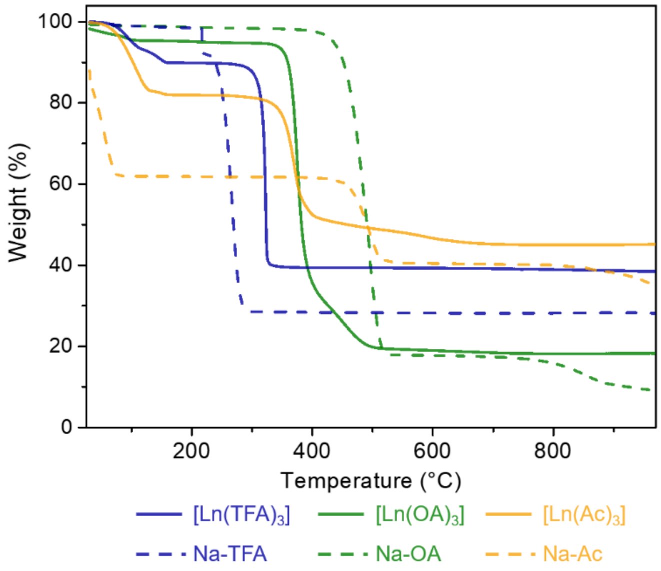

Figure S5. TGA profiles of each of the Ln^{3+} precursors as well as sodium sources used in the microwave-assisted thermal decomposition.

The thermal decomposition profiles of the three Ln-precursors showed a first weight loss of up to 10% at temperatures below 200 °C. This was attributed to the removal of residual water and trifluoracetic acid, while the actual thermal decomposition took place at higher temperatures. The steep decrease in weight obtained for $[Ln(TFA)_3]$ indicated a decomposition temperature of 320 °C, which matches well with data reported in the literature.[1-2] In contrast, the main decomposition step of $[Ln(OA)_3]$ and $[Ln(Ac)_3]$ was found to be shifted towards higher temperatures, namely 380 °C.[3-4] Moreover, both of the latter precursors exhibited a second, less pronounced mass loss at higher temperatures. Based on reported literature, these two weight losses correspond to the decomposition of the anhydrous precursor to the oxycarbonate, $Ln_2O_3 \cdot CO_2$, as well as the formation of the sesquioxide, Ln_2O_3.[4] In addition to the Ln-precursors, we investigated the thermal decomposition behaviour of the used sodium sources. The decomposition profile obtained for Na-TFA showed a steep mass decrease at 280 °C. Thus, Na-TFA decomposed at lower temperatures when compared to $[Ln(TFA)_3]$. In contrast, for both Na-OA and Na-Ac, decomposition took place at a temperature exceeding that of the decomposition temperature of their Ln analogues, namely at 490 °C.

It must be taken into account that the data shown here were obtained upon thermal decomposition of the precursors in their solid state under nitrogen, whereas the microwave-assisted NP synthesis took place in solution and in the presence of additional ligands (namely oleylamine and/or oleic acid). Therefore, decomposition temperatures in the microwave-assisted reactions differed from those observed by TGA. Nonetheless, trends seen here provide strong evidence that the formation of larger-size NPs utilizing $[Ln(TFA)_3]$ *versus* smaller-size NPs from $[Ln(OA)_3]$ and $[Ln(Ac)_3]$ are in line with the thermal stability of the precursors. Overall, this demonstrates that careful selection of precursors exhibiting different chemistry offers an interesting mean towards controlled NP growth.

6. Precursor-Dependent Pressure Profiles during the Microwave Reaction

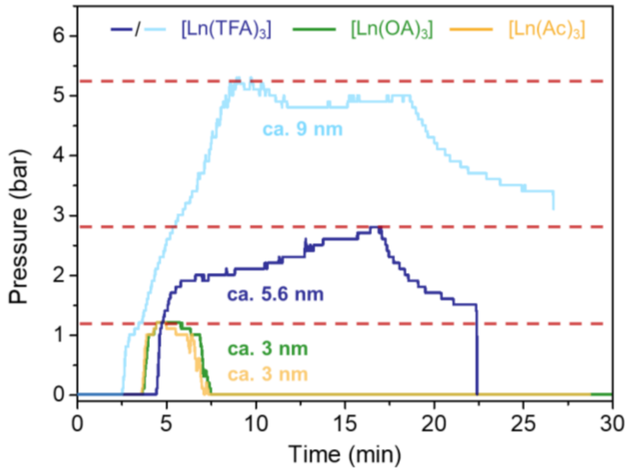

Figure S6. Profiles showing the time-dependent pressure evolution during the microwave-assisted synthesis of cubic (light blue line) and hexagonal (dark blue, green, yellow lines) $NaGdF_4$:Yb^{3+},Er^{3+} NPs using [$Ln(TFA)_3$], [$Ln(OA)_3$], and [$Ln(Ac)_3$] as precursors. Herein, given pressure values constitute the pressure that was sensed on the Teflon cap placed on the microwave reaction vessel. In the figure are also included the approximated sizes of the resulting NPs for each synthesis.

As the microwave-assisted synthesis of NPs takes place in a closed system, increase in temperature, decomposition of precursors and formation of gaseous by-products resulted in pressure increase in the microwave reaction vessels. Herein, the obtained pressure profiles showed distinct characteristics for [$Ln(TFA)_3$] on one side and [$Ln(OA)_3$] and [$Ln(Ac)_3$] on the other side (Figure S6).

For all precursors, pressure steeply increased at the beginning of the reaction with increasing temperature during the first 5 min. This rise in pressure was associated with the beginning of the precursor decomposition, triggering the formation of first nuclei. Notably, the pressure profiles in case of [$Ln(OA)_3$] and [$Ln(Ac)_3$] were very similar to each other, and the pressure increase reached its maximum of 1.3 bar within less than 5 min. The pressure remained unchanged till 7 min – the time point at which the set reaction temperature was approached –, followed by a drop to atmospheric pressure (pressure applied to the Teflon cap: 0 bar) for the remaining reaction time. It can be noted that such a pressure profile exhibits a LaMer-like character.[5-7] Therefore, it is suggested that the temperature-induced increase in pressure also reflects a growing precursor decomposition rate, along with increasing nucleation that in turn reached its maximum at maximum pressure. Meanwhile, for [$Ln(TFA)_3$], the pressure rose continuously during the complete reaction time and increased by maximum values of 2.8 and 5.3 bar, respectively, before decreasing to atmospheric pressure upon initialization of the cooling process. Along with these higher-pressure conditions during the reaction came larger NP sizes of ca. 5.6 and 9 nm, respectively (compared to only ca. 3 nm for [$Ln(OA)_3$] and [$Ln(Ac)_3$]). Among the two samples prepared using [$Ln(TFA)_3$], larger reaction pressure could be correlated with larger particle size.

We further found that NP growth was less time-sensitive when [$Ln(OA)_3$] was utilized as precursor in comparison to [$Ln(TFA)_3$] (*vide infra*, Figure S14). Almost no size increase was observed in case of [$Ln(OA)_3$] when the reaction time was prolonged from 1 min (ca. 3 nm) to 10 min (ca. 3.2 nm). Yet, when [$Ln(TFA)_3$] was employed, a more sizeable increase from ca. 4.5 nm after 1 min to ca. 5.6 nm after 10 min reaction time was determined. The latter can be ascribed to the continuously increasing pressure within the vessel triggering ongoing precursor decomposition and particle growth. In case of the former, nucleation processes terminated at an earlier reaction stage as indicated by the pressure decrease down to atmospheric pressure, followed by only minor particle growth by diffusion.

Thus, overall, the here observed differences in the pressure profiles for [Ln(OA)$_3$] and [Ln(Ac)$_3$] *versus* [Ln(TFA)$_3$] further indicate that precursor chemistry has a strong influence on the nucleation and particle growth mechanism, ultimately yielding either sub-10 nm or sub-5 nm NaGdF$_4$:Yb^{3+},Er^{3+} NPs.

7. Excited State Lifetime Measurements

Due to the complex nature of the upconversion emission process in Ln-NPs, the luminescence decay curves shown below do not have a clear single-exponential character.[8-9] The Yb^{3+}-to-Er^{3+} energy transfer rate, the lifetime of Er^{3+} intermediate levels and the lifetime of Yb^{3+} excited state (which play a role in the upconversion excitation pathway) may influence the emitting level decay profile.[8] Moreover, these small Ln-NPs likely have emission centres occupying sites with different chemical surroundings and coordination environments (namely at the NP surface and in the NP core), resulting in a heterogeneous population of the emitting Ln^{3+} ions.[10] Accounting for this heterogeneity (reflected in the multi-exponential character of the decay curves), we determined the lifetimes of the $^4S_{3/2}$ and $^4F_{9/2}$ emitting levels of Er^{3+} by integration of the area under the normalized emission decay curves. The lifetime values obtained by this method, for each of the decay curves shown in Figures S7 to S9, are given in the Table S2.

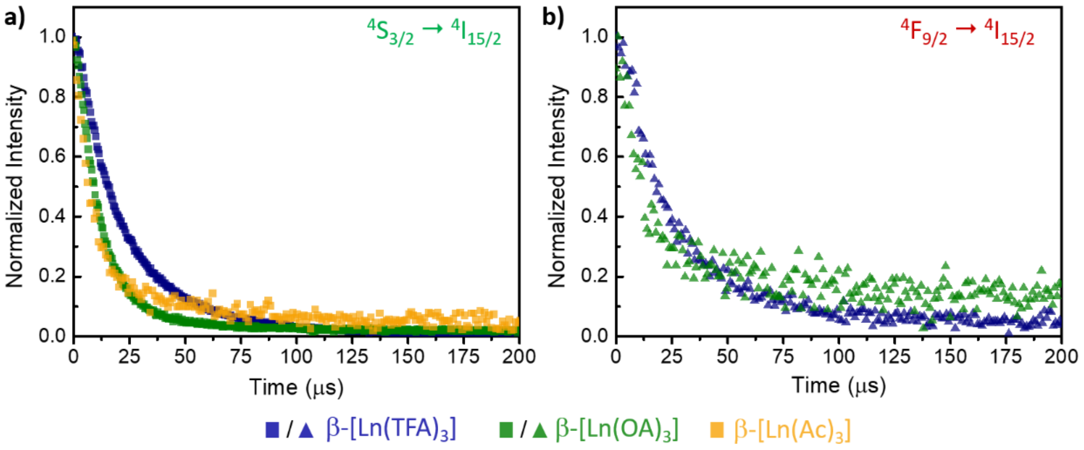

Figure S7. Decay curves of the a) $^4S_{3/2} \rightarrow {}^4I_{15/2}$ (540 nm) and b) $^4F_{9/2} \rightarrow {}^4I_{15/2}$ (650 nm) Er^{3+} transitions for β-$NaGdF_4$:Yb^{3+},Er^{3+} NPs synthesized using [Ln(TFA)$_3$], [Ln(OA)$_3$], and [Ln(Ac)$_3$] as precursors. All decay curves were obtained under 980 nm pulsed laser excitation.

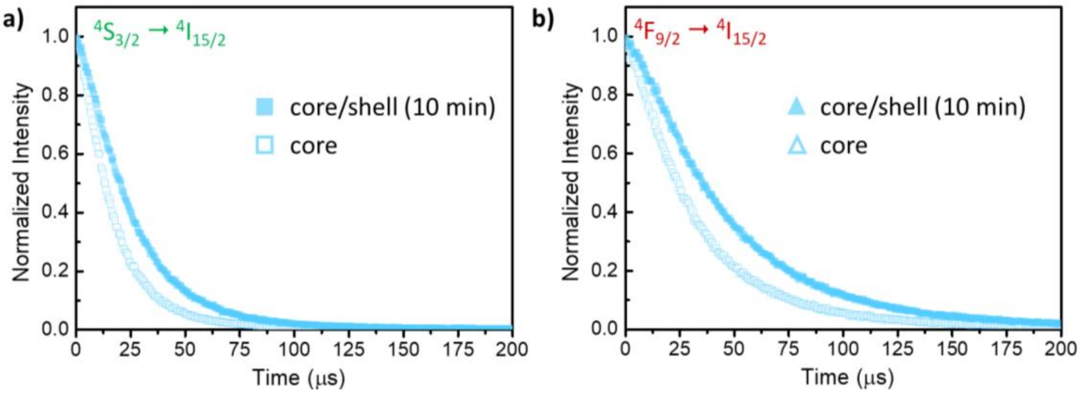

Figure S8. Decay curves of the $^4S_{3/2} \rightarrow {}^4I_{15/2}$ (540 nm) and $^4F_{9/2} \rightarrow {}^4I_{15/2}$ (650 nm) Er^{3+} transitions for α-$NaGdF_4$:Yb^{3+},Er^{3+} core-only and core/shell NPs synthesized using [Ln(TFA)$_3$] precursors. The decay curves were obtained under 980 nm pulsed laser excitation.

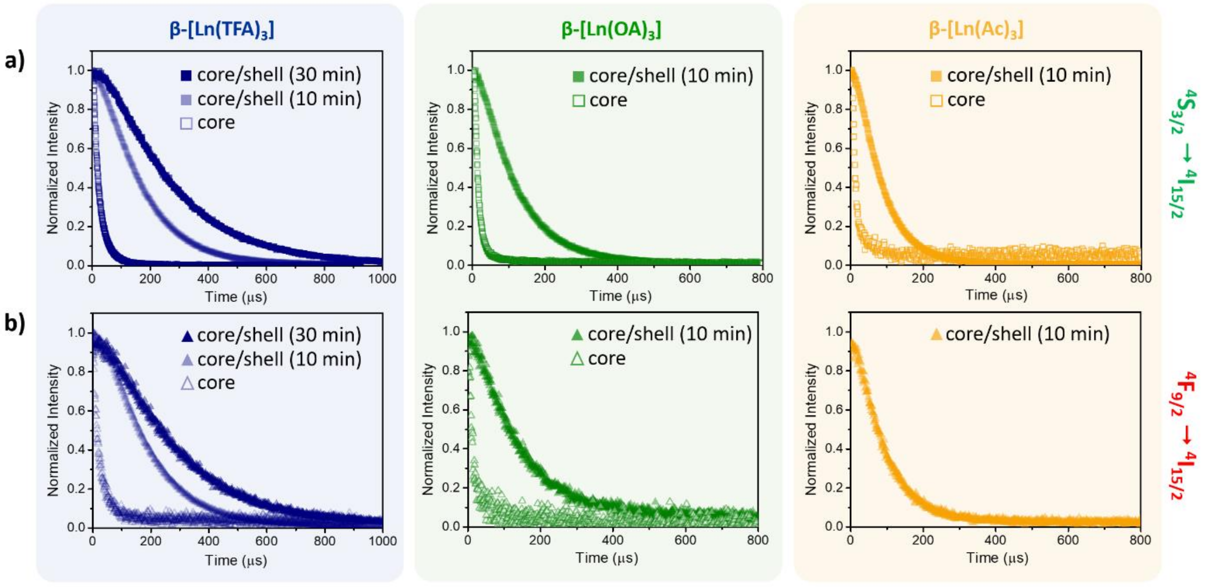

Figure S9. Decay curves of the a) $^4S_{3/2} \rightarrow {}^4I_{15/2}$ (540 nm) and b) $^4F_{9/2} \rightarrow {}^4I_{15/2}$ (650 nm) transitions for core-only and core/shell β-$NaGdF_4$:Yb^{3+},Er^{3+} NPs synthesized using [Ln(TFA)$_3$], [Ln(OA)$_3$], and [Ln(Ac)$_3$] as precursors. All decay curves were obtained under 980 nm pulsed laser excitation.

Table S2. Lifetime values, corresponding NP sizes and shell thicknesses of α- and β-$NaGdF_4$:Yb^{3+},Er^{3+} core-only and core/shell NPs synthesized by the microwave-assisted method.

Type of NP	Core Precursor [a]	Crystal Phase	Lifetime (μs)		Approx. NP Size (nm)	Shell Thickness (nm)
			$^4S_{3/2} \rightarrow {}^4I_{15/2}$ [540 nm]	$^4F_{9/2} \rightarrow {}^4I_{15/2}$ [655 nm]		
Core-only	[Ln(TFA)$_3$]	β	22	25	5.5	0
	[Ln(OA)$_3$]		16	18	3.0	
	[Ln(Ac)$_3$]		17	– [b]	3.0	
	[Ln(TFA)$_3$]	α	15	29	9.3	0
Core/Shell (10 min shell)	[Ln(TFA)$_3$]	β	156	156	11.8	2.5
	[Ln(OA)$_3$]		103	127	6.8	2.2
	[Ln(Ac)$_3$]		73	87	5.6	1.4
	[Ln(TFA)$_3$]	α	25	43	11.3	1.0
Core/Shell (30 min shell)	[Ln(TFA)$_3$]	β	259	260	15.5	4.1

[a] For shell growth, [Ln(TFA)$_3$] was used as precursor.

[b] Weak emission band.

8. Additional Optical Characterization

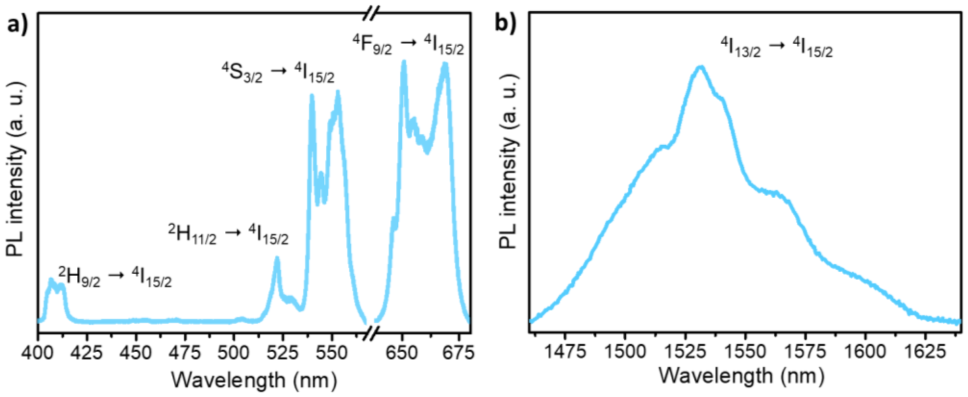

Figure S10. a) Upconversion and b) NIR emission spectra of α-NaGdF$_4$:Yb^{3+},Er^{3+} NPs obtained by the microwave-assisted decomposition of [Ln(TFA)$_3$]. All spectra were obtained under 980 nm laser excitation (*P* = 150 mW).

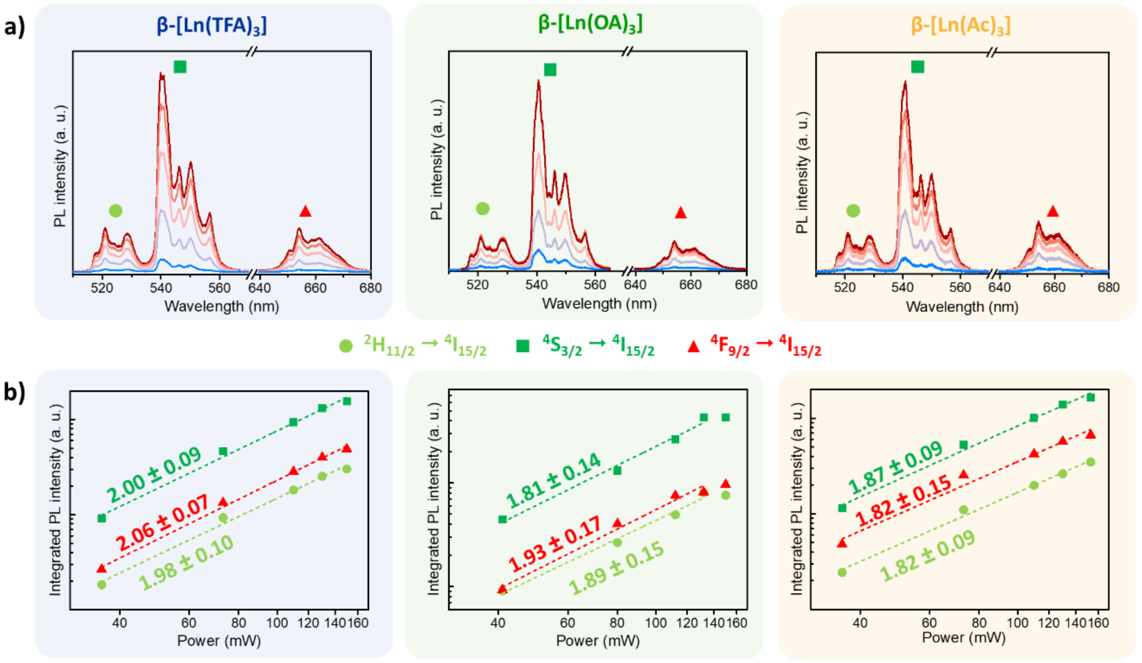

Figure S11. a) Excitation power-dependent upconversion spectra, and b) integrated $^2H_{11/2} \rightarrow {}^4I_{15/2}$, $^4S_{3/2} \rightarrow {}^4I_{15/2}$, and $^4F_{9/2} \rightarrow {}^4I_{15/2}$ Er^{3+} emissions *vs* 980 nm excitation power density for β-NaGdF$_4$:Yb^{3+},Er^{3+} NPs synthesized using [Ln(TFA)$_3$], [Ln(OA)$_3$], and [Ln(Ac)$_3$].

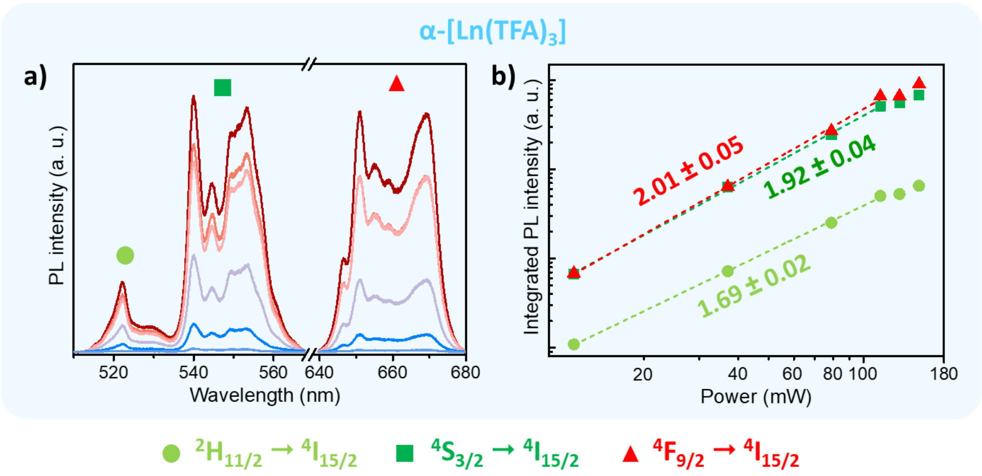

Figure S12. a) Excitation power-dependent upconversion spectra, and b) integrated $^2H_{11/2} \rightarrow {}^4I_{15/2}$, $^4S_{3/2} \rightarrow {}^4I_{15/2}$, and $^4F_{9/2} \rightarrow {}^4I_{15/2}$ Er^{3+} emissions *vs* 980 nm excitation power density for α-$NaGdF_4$:Yb^{3+},Er^{3+} NPs synthesized using [$Ln(TFA)_3$] as precursor.

9. Effect of Reaction Time and Temperature on Crystalline Phase, Size, and Photoluminescence

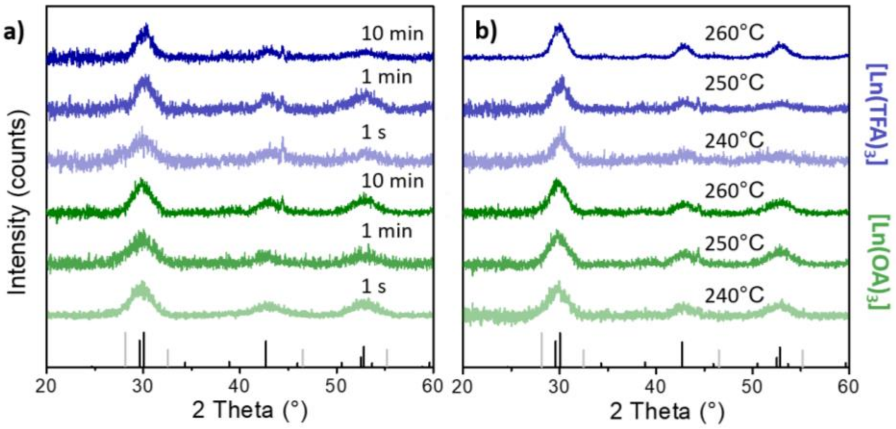

Figure S13. Effect of reaction time and temperature on the crystalline phase of NPs obtained from [Ln(TFA)$_3$] and [Ln(OA)$_3$]: a) XRD patterns of NPs obtained after 1 s, 1 min, and 10 min, respectively (Reaction temperature: T_1 = 260 °C, T_2 = 250 °C). b) XRD patterns of NPs obtained at different reaction temperatures T_2 (Reaction time: 10 min). References: β-NaGdF$_4$ (PDF#: 01-080-8787, black lines), α-NaGdF$_4$ (PDF#: 00-027-0697, light grey lines).

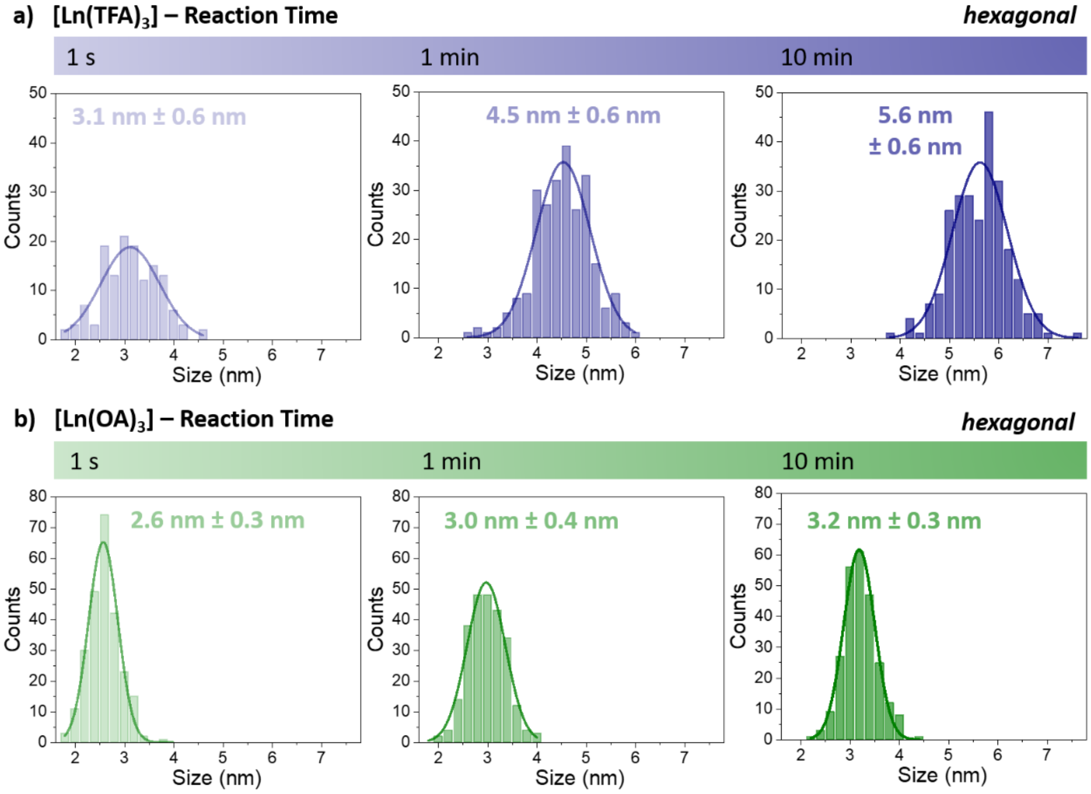

Figure S14. Influence of the reaction time on mean size and size distribution of β-NaGdF$_4$:Yb^{3+},Er^{3+} NPs synthesized using a) [Ln(TFA)$_3$] and b) [Ln(OA)$_3$] as precursors. Reaction times varied between 1 s and 10 min as indicated in the figure. Reaction temperature T_2: 250 °C. The Na$^+$-to-Ln^{3+} ion ratio was set aiming for the hexagonal crystalline phase.

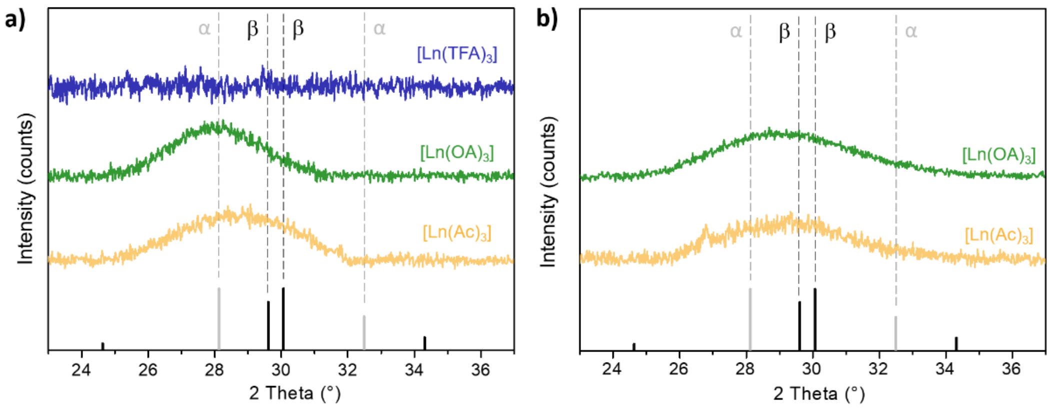

Figure S15. Assessment of the crystalline phase formation during the synthesis of β-$NaGdF_4$:Yb^{3+},Er^{3+} NPs. XRD patterns are shown for samples obtained using [$Ln(TFA)_3$], [$Ln(OA)_3$] and [$Ln(Ac)_3$] as precursors. a) The reactions were stopped shortly after the start, namely when reaching a temperature of 200 °C and a pressure of ca. 1 bar. b) Using [$Ln(OA)_3$] and [$Ln(Ac)_3$] as precursors, the reactions were kept at 200 °C for 10 min. References: α-$NaGdF_4$ (PDF#: 00-027-0697, light grey lines), β-$NaGdF_4$ (PDF#: 01-080-8787, black lines). Dashed lines are guides for the eye marking the position of the main reflections of the cubic and the hexagonal phase, respectively.

XRD patterns shown in Figure S15a reveal that, at lower temperatures, no phase-pure cubic NPs could be isolated. In case of [$Ln(TFA)_3$], no crystalline product was obtained at all. Stopping the reaction at 230 °C (data not shown) did not yield any crystalline phase either. In case of [$Ln(OA)_3$] and [$Ln(Ac)_3$], the broad peaks indicate the presence of a phase mixture. Here, the contribution of the hexagonal phase can be estimated to be more pronounced for [$Ln(Ac)_3$]-derived NPs (broad peak more shifted towards the hexagonal reference) than for [$Ln(OA)_3$]-based NPs (broad peak more shifted towards the cubic reference). This indicates that both precursors, [$Ln(OA)_3$] and [$Ln(Ac)_3$], enable the formation of the hexagonal crystal phase already at an early stage of the reaction – [$Ln(Ac)_3$] promoting more the hexagonal phase formation. Similar results were obtained when the reaction time was prolonged to 10 min (200 °C, Figure S15b), indicating that the reaction *temperature* has greater influence on the α → β phase transformation than the reaction *time*.

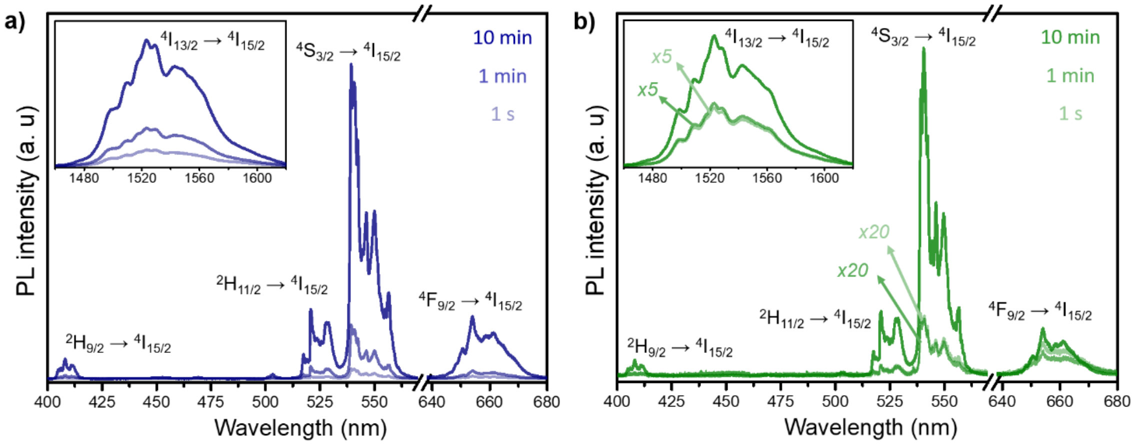

Figure S16. Influence of the reaction time on the visible and NIR (inset) photoluminescence upon 980 nm excitation of NPs synthesized using a) [$Ln(TFA)_3$] and b) [$Ln(OA)_3$] as precursors. Reaction temperature T_2: 250 °C. The Na^+-to-Ln^{3+} ion ratio was set to obtain the hexagonal phase.

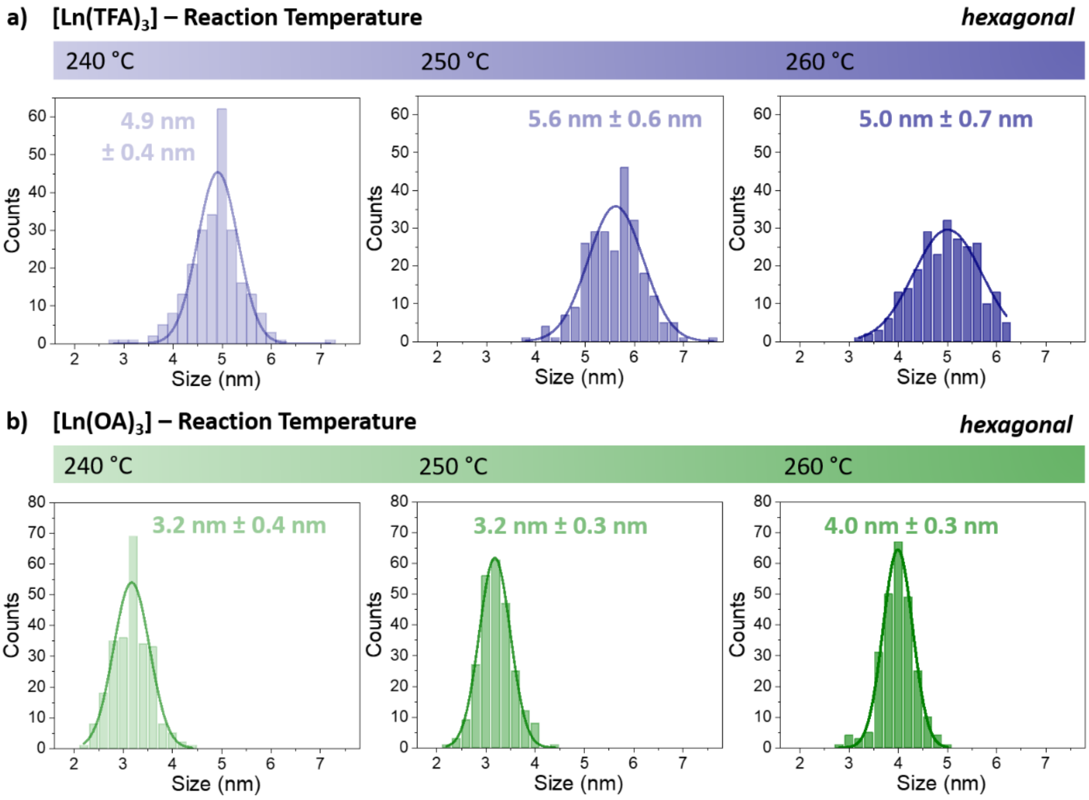

Figure S17. Influence of the reaction temperature (T_2) on mean size and size distribution of NaGdF$_4$:Yb^{3+},Er^{3+} NPs synthesized using a) [Ln(TFA)$_3$] and b) [Ln(OA)$_3$] as precursors. Reaction time: 10 min. The Na$^+$-to-Ln^{3+} ion ratio was set aiming for the hexagonal crystalline phase.

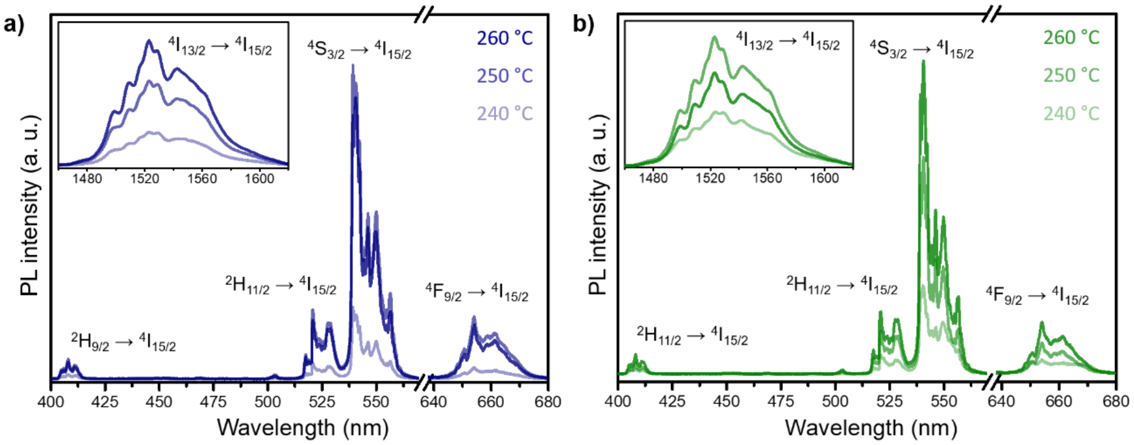

Figure S18. Influence of the reaction temperature on the visible and NIR (inset) photoluminescence upon 980 nm excitation of NPs synthesized using a) [Ln(TFA)$_3$] and b) [Ln(OA)$_3$] as precursors. Reaction time was t_2: 10 min. The Na$^+$-to-Ln^{3+} ion ratio was set to obtain the hexagonal phase.

10. Upconversion and NIR Luminescence Enhancement through Shell Growth

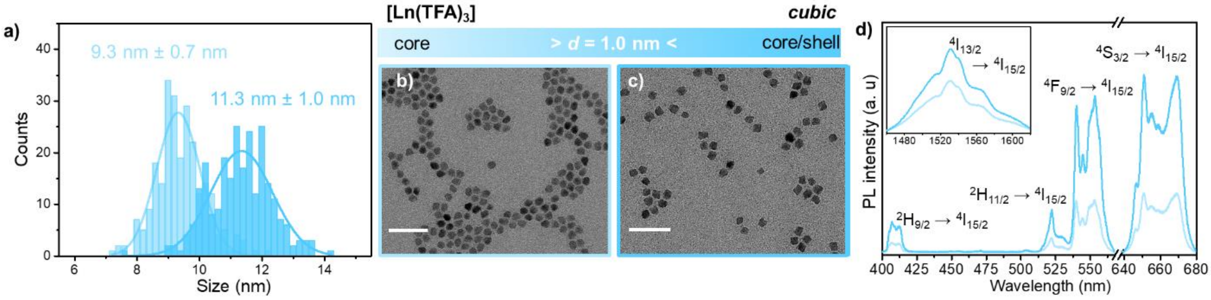

Figure S19. a) Size distribution of core-only and core/shell cubic-phase NPs: cores and shells were grown using $[Ln(TFA)_3]$ as precursors. b and c) Corresponding TEM images of core-only as well as core/shell NPs. d) Associated photoluminescence in the visible and NIR (inset) spectral regions. Reaction temperatures: 230 °C for core and shell growth each. Reaction time: 10 min for core and shell growth each. Scale bars in TEM images are 50 nm.

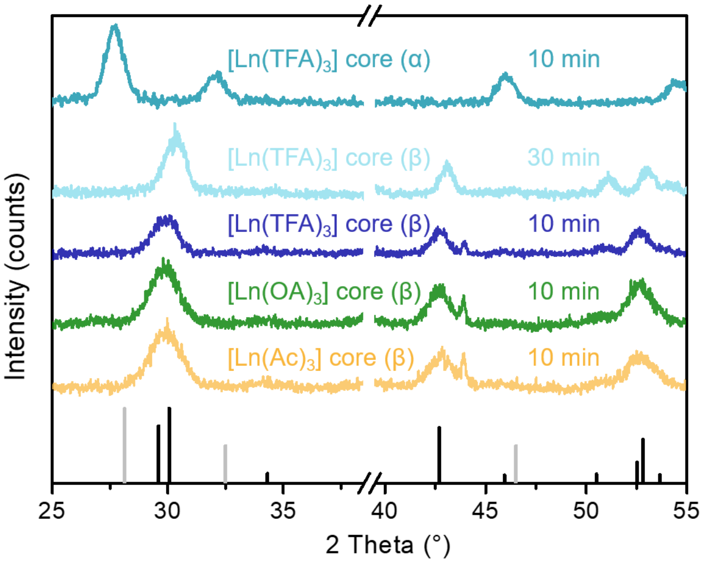

Figure S20. XRD patterns of core/shell NPs. The shells were grown using $[Ln(TFA)_3]$ as precursor within 10 min on $[Ln(TFA)_3]$-, $[Ln(OA)_3]$-, and $[Ln(Ac)_3]$-derived NPs. The figure also shows the XRD pattern obtained on NPs with a thick shell grown for 30 min (core- and shell-precursor: $[Ln(TFA)_3]$). Reference: α-$NaGdF_4$ (PDF#: 00-027-0697, light grey lines), β-$NaGdF_4$ (PDF#: 01-080-8787, black lines). Reflections at 39° due to NaF were removed for clarity. The reflection at 44° is due to the sample holder.

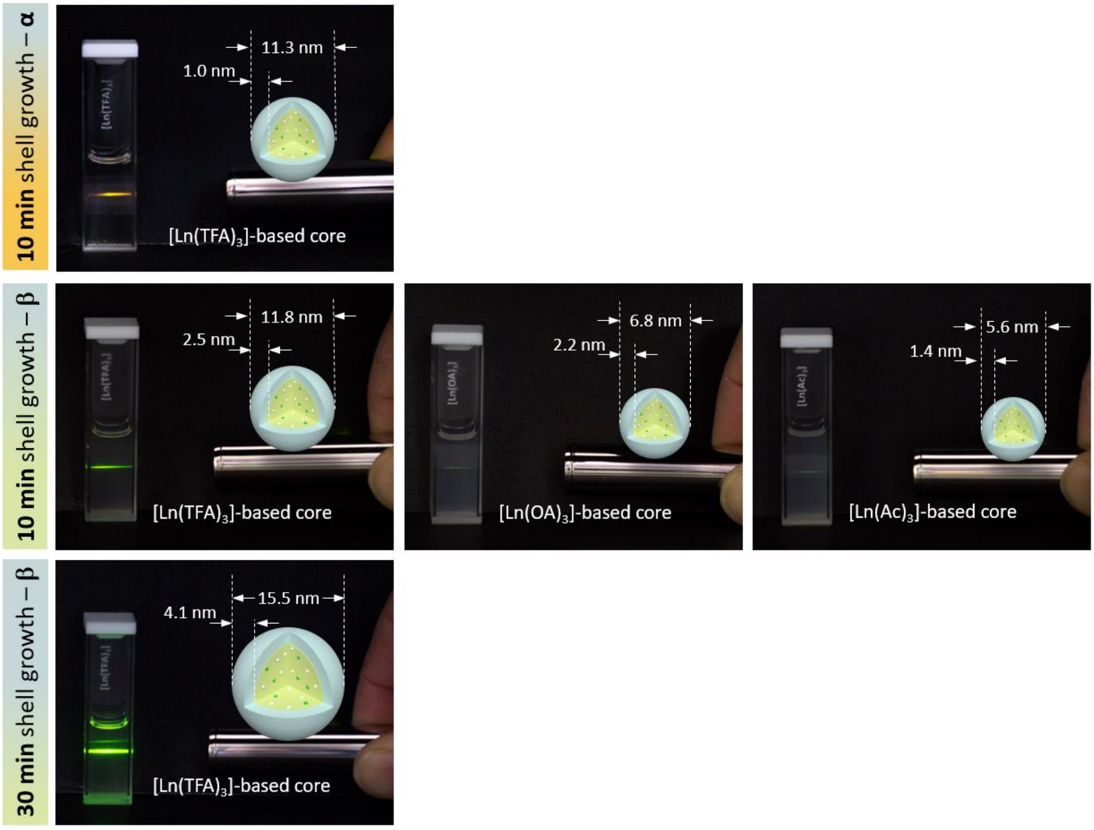

Figure S21. Photographs of α- and β-$NaGdF_4$:Yb^{3+},Er^{3+}/$NaGdF_4$ core/shell NPs dispersed in toluene under excitation with a 980 nm 50 mW laser pointer. Upper row (cubic phase): As expected, growth of a shell on [Ln(TFA)$_3$]-derived cubic-phase cores resulted in upconversion enhancement yielding bright orange emission (NP concentration: 16 mg/mL). Middle row (hexagonal phase): $NaGdF_4$ shells were grown within 10 min of microwave irradiation using [Ln(TFA)$_3$] as precursor subsequent to core synthesis employing [Ln(TFA)$_3$], [Ln(OA)$_3$], and [Ln(Ac)$_3$] (left to right). Brighter green upconversion emission was observed with increasing particle size. Note that the NP concentrations of the samples based on [Ln(OA)$_3$]- and [Ln(Ac)$_3$]-derived cores were augmented to 25.5 mg/mL and 38.0 mg/mL, respectively, to allow for visualization of the upconversion emission. In case of larger [Ln(TFA)$_3$]-derived samples, the NP concentration was 16 mg/mL. Lower row (hexagonal phase): Growth of a thicker shell on [Ln(TFA)$_3$]-derived cores resulted in further upconversion enhancement (NP concentration: 16 mg/mL).

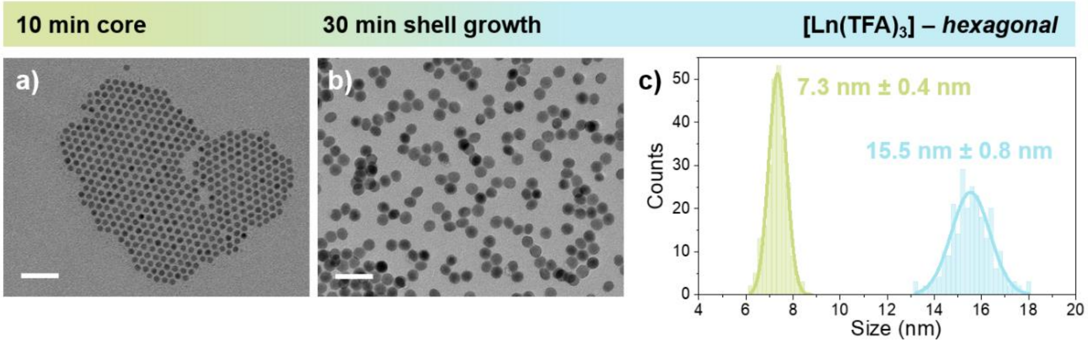

Figure S22. TEM images of β-$NaGdF_4$:Yb^{3+},Er^{3+} NPs a) before and b) after the growth of a $NaGdF_4$ shell. [Ln(TFA)$_3$] was used as precursor for both core and shell. c) Size distribution of the NPs shown in a) and b). Scale bars in the TEM images: 50 nm.

Seeking real-life applications, brightness of the upconverted emission is one important aspect. In addition, the possibility to trigger emission by simple means of excitation – *i.e.* without the need for a sophisticated set-up – can constitute a further asset. In the aim of this, we assessed the upconversion emission from core/shell UCNPs under excitation with a hand-hold NIR laser pointer.[※] Remarkably, despite their small size – sub-10 nm in case of [Ln(OA)$_3$]- and [Ln(Ac)$_3$]-derived core/shell NPs, sub-15 nm in case of [Ln(TFA)$_3$]-derived core/shell NPs (Figure S21, upper and middle row) –, the α-phase sample exhibited orange and all β-phase samples showed green upconversion emission, visible by naked eye. As expected, dispersions of higher NP concentration were required in case of the sub-10 nm UCNPs, while bright emission was obtained from the larger, ca. 11 nm and 12 nm sized sample, even at lower concentration.

The photograph shown in the lower row of Figure S21 demonstrates that further upconversion enhancement was achievable by growing a thicker – ca. 4 nm – shell around the [Ln(TFA)$_3$]-derived hexagonal core, while retaining a size of less than 20 nm (Figure S22). For this, the same reaction settings were applied as for the thinner shell, however, reaction time for shell growth was prolonged to 30 min. Similarly, Resch-Genger *et al.* reported an optimized shell thickness of 5 nm for ultrasmall NPs (obtained by a conventional decomposition approach) exhibiting both optimized upconversion and NIR emission.[9] Thus, the here shown brightly emitting $NaGdF_4$:Yb^{3+},Er^{3+}/$NaGdF_4$ core/shell NPs validate the suitability of the developed microwave-assisted route as rapid alternative to conventional strategies towards small and ultrasmall Ln-NPs.

[※] 980 nm, 50 mW laser pointer (focused at 2 cm) by Roithner Lasertechnik GmbH, Vienna, Austria.

11. References

1 H. Eloussifi, J. Farjas, P. Roura, J. Camps, M. Dammak, S. Ricart, T. Puig and X. Obradors, *J. Therm. Anal. Calorim.,* 2012, **108**, 589.

2 S. Mishra, L. G. Hubert-Pfalzgraf, S. Daniele, M. Rolland, E. Jeanneau and B. Jouguet, *Inorg. Chem. Commun.,* 2009, **12**, 97.

3 E. Hemmer, Y. Kohl, V. Colquhoun, H. Thielecke, K. Soga and S. Mathur, *J. Phys. Chem. B,* 2010, **114**, 4358.

4 K. Patil, G. Chandrashekar, M. George and C. Rao, *Can. J. Chem.,* 1968, **46**, 257.

5 V. K. LaMer and R. H. Dinegar, *J. Am. Chem. Soc.,* 1950, **72**, 4847.

6 V. K. LaMer, *Ind. Eng. Chem.,* 1952, **44**, 1270.

7 N. T. K. Thanh, N. Maclean and S. Mahiddine, *Chem. Rev.,* 2014, **114**, 7610.

8 J. Bergstrand, Q. Liu, B. Huang, X. Peng, C. Würth, U. Resch-Genger, Q. Zhan, J. Widengren, H. Ågren and H. Liu, *Nanoscale,* 2019, **11**, 4959.

9 C. Würth, S. Fischer, B. Grauel, A. P. Alivisatos and U. Resch-Genger, *J. Am. Chem. Soc.,* 2018, **140**, 4922.

10 S. Bhuckory, E. Hemmer, Y.-T. Wu, A. Yahia-Ammar, F. Vetrone and N. Hildebrandt, *Eur. J. Inorg. Chem.,* 2017, **2017**, 5186.